PAPER • OPEN ACCESS

Flexible correction of 3D non-linear drift in SPM measurements by data fusion

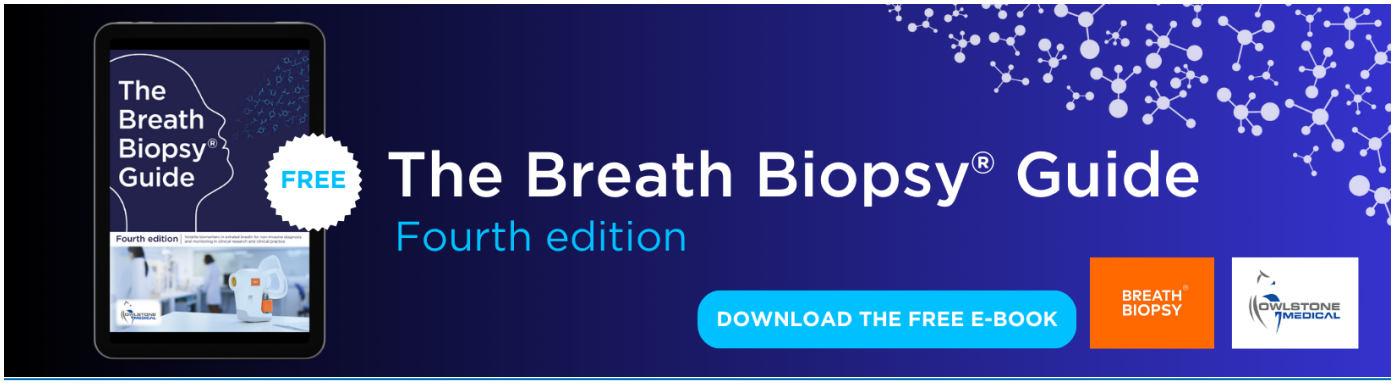

OPEN ACCESS
IOP Publishing
Measurement Science and Technology
Meas. Sci. Technol. **32** (2021) 035005 (11pp)
https://doi.org/10.1088/1361-6501/abc9f8

Flexible correction of 3D non-linear drift in SPM measurements by data fusion

Johannes Degenhardt[1], **Rainer Tutsch**[2] **and Gaoliang Dai**[1]

[1] Physikalisch-Technische Bundesanstalt, Bundesallee 100, Braunschweig 38116, Germany
[2] Technische Universität Braunschweig, IPROM, Schleinitzstraße 20, Braunschweig 38106, Germany

E-mail: Gaoliang.Dai@ptb.de

Received 7 September 2020, revised 26 October 2020
Accepted for publication 12 November 2020
Published 11 December 2020

Abstract

In this article a new offline method for correcting non-linear drift in all three dimensions (3D) is presented. Using this method, a sample region is measured in multiple sub-measurements, each with increased sampling distance and thus reduced measurement time. The datasets of the sub-measurements are aligned using a point-to-plane iterative closest point algorithm to reconstruct and correct the 3D drift. Afterwards, the corrected datasets are fused into a single dataset. Compared to conventional drift-correction methods, the new method has the advantages of drift correction in full 3D with higher temporal resolution, less extra measurement time and data redundancy, as well as high application flexibility (e.g. compatibility to non-raster sampling). However, the resulting dataset might have slightly decreased resolution. If a high-resolution low-drift dataset is required, the method can be applied in an extended way, where an additional high-resolution measurement is taken whose drift can be corrected by the aforementioned dataset generated by data fusion. Two experimental measurements and a simulation study have been carried out in a new low-noise 3D atomic force microscope, showing great application potential of the proposed method.

Keywords: drift correction, scanning probe microscopy (SPM), 3D-nanometrology, data fusion, iterative closest point (ICP) algorithm

(Some figures may appear in colour only in the online journal)

1. Introduction

Thermal drift is a common problem in precision measurements, particularly in scanning probe microscopes (SPMs) due to their low measurement speed. In an atomic force microscope (AFM), which is the most widely used type of SPM, and which we will therefore focus on in this article, drift is an uncontrolled relative motion of the tip and a sample, usually caused by thermal expansion. To reduce the thermal drift in AFM (and other SPMs) it is thus a straightforward idea to use hardware measures, e.g. constructing an AFM measurement chain with low thermal expansion materials, with low temperature variation (active/passive heating/cooling, installation in a climatized room/inside a thermal insulation chamber, high thermal mass of the components, etc) [1–4], and making an AFM as small as possible. In addition, measures are taken to optimize the mechanical construction so that the thermal expansions of different components compensate each other. A typical way is to design the structure symmetrically and to match the thermal expansion coefficients of the applied materials carefully [5]. However, hardware measures are usually expensive or may be unfeasible. If the drift is not satisfying, even if hardware measures are exhausted, alternative software-based drift-correction methods are needed.

Drift correction can be performed either online or offline. Online correction measures the drift during measurements and corrects it *in situ* by adding offsets to the scanner deflections;

thus, its acquired raw data are drift-corrected. However, its implementation is not always feasible because it needs access to the measurement software and/or scan controller. Furthermore, the drift must be detected precisely for correction, either using additional sensors [6] or the AFM itself. If additional sensors are applied for drift detection, their noise and resolution may significantly impact the AFM measurements. On the other hand, if the AFM is applied for drift detection, it has to switch between the tasks of normal measurement and drift detection [7], or scan consecutive images [8] or overlapping image segments to calculate drift. The detected drift is input into a drift model, e.g. a linear model [7] or a neural network [8], for online prediction and correction of drift during the normal measurement.

Offline correction methods correct the drift in measured raw datasets after a measurement is finished. Thus, they avoid the need to access the measurement system or predict future drift. Different offline drift-correction methods have been proposed. The advantages and disadvantages of some contemporary methods are summarized in table 1, where these methods are evaluated from the aspects of the axes in which the drift is corrected, their performance, their cost and their application flexibility.

Marinello *et al* [9] and Meyer *et al* [10] correct vertical drift in AFM data with high temporal resolution. Marinello *et al* scan a raster image and consecutively rescan a narrow strip of the image with the fast measurement axis orientated orthogonal to the previous one. Assuming that drift along a scan line can be neglected, they realign the scanlines of the original image in the z-axis to the lines of the rescanned strip. Meyer *et al* use a spiral scan path, which self-intersects multiple times during a single measurement. The measured heights at the intersecting data points are used to determine the course of the z-drift and subsequently to correct it. Both methods have high temporal drift resolution and require a small amount of redundant data for the drift correction. However, the methods are limited to the correction of z-drift only.

Kizu *et al* [11] correct drift along the z-axis and the fast measurement axis. After each single 'normal' scanline acquired over a line structure, they rescan the first scan line of the measurement. Then, they use an iterative closest point (ICP) algorithm to align the first scan line and the rescanned 'first' lines to obtain their drift caused offsets and then correct the 'normal' scan lines using the detected drift. Their method has shown excellent drift-correction performance of about 1 nm due to small temporal drift resolution (i.e. twice the time needed for a scan line). However, the method is limited to drift correction in the z- and the fast scan axes only. Furthermore, the method is limited to measurements of line features, thus lacking application flexibility.

Methods for correcting 3D drift have been proposed by several authors. Lapshin [13] uses pairs of 'counter-scanned images (CSI)' to calculate and correct linear 3D drift. The drift is determined by calculating the offset of the same surface features measured in images of a CSI pair. This method needs doubled measurement time and has poor temporal drift resolution; however, the noise in the measured data is reduced by averaging the corrected images. Rahe *et al* [12] proposed a correction method that is similar to that of Lapshin. While Lapshin works with images in which the scan directions got reversed, Rahe *et al* use images obtained under constant scan directions. With a sufficient number of consecutively scanned images, the approach of Rahe *et al* can be extended to correct non-linear drift. However, the drawbacks of this method are similar to that of Lapshin.

Follin *et al* [14] rescan a slightly larger image sliver than Marinello *et al* do (i.e. higher data redundancy) to correct 3D drift. They model the drift as third-order polynomials and determine the coefficients of the drift model through a search algorithm, finding the coefficients that minimize the differences between the corrected image and sliver. As the remeasurement is applied on a sliver instead of a complete image, it thus has reduced data redundancy and increased temporal resolution.

In this paper, we propose a new offline drift-correction method based on modern data fusion using the point-to-plane ICP algorithm. Compared to the aforementioned methods, it has the advantages of high temporal drift resolution, principally without data redundancy and thus potentially little additional measurement time, as well as applicability to various measurement tasks. The concept, realization, experimental and simulation studies of this new method will be detailed in this paper.

2. Concept

The principle of the new drift-correction method is illustrated in figure 1. Using this method, a desired measurement is split into multiple consecutive sub-measurements (marked as 1, 2, 3, …, N). These sub-measurements have (almost) the same measurement area, but an increased sampling distance and thus a reduced point number than the original measurement. The locations of the sub-measurement areas are intentionally shifted with each other, so that the collected data points of all the sub-measurements can well represent that of the original measurement task. After all the sub-measurements have been taken, their point clouds are aligned with each other in 3D using a point-to-plane ICP algorithm [15], which will be detailed later. The determined 3D offsets of the datasets in the alignment processes represent the 3D drifts of the sub-measurements. A temporal drift curve (i.e. drift vs time) for the x, y and z-axes can then be reconstructed based on the determined 3D offsets and the timestamps of sub-measurements. Using this curve, the drifts of all data points in all sub-measurements can be corrected and, finally, they can be merged to generate a complete and drift-corrected AFM image for the desired measurement task.

It should be mentioned that the pixel-wise splitting concept shown in figure 1 is suitable for AFMs using a pixel-by-pixel measurement strategy, such as the peak-force [16] or vector approaching probing (VAP) [17] methods. In such AFMs, the needed measurement time is almost proportional to the number of measurement points. As the tip and sample are not in contact during the horizontal positioning steps using such measurement strategies no additional tip wear is to be

Table 1. A summary of different offline drift-correction methods regarding the axes of drift correction, the performance concerning temporal resolution, the costs concerning the extra measurement time and/or the data redundancy needed, and its application flexibility (fsa = fast scan axis).

Method	Axes		Performance, i.e. temporal drift resolution	Cost, i.e. extra measurement time/data redundancy	Applicability/Flexibility
Marinello *et al* [9]	z	−	++	+	0
Meyer *et al* [10]	z	−	++	+	−
Kizu *et al* [11]	z, fsa	0	++	−	−−
Rahe *et al* [12]	x, y, z	++	−	−−	0
Lapshin [13]	x, y, z	++	−	−	0
Follin *et al* [14]	x, y, z	++	0	0	0
New method	x, y, z	++	+	+	+

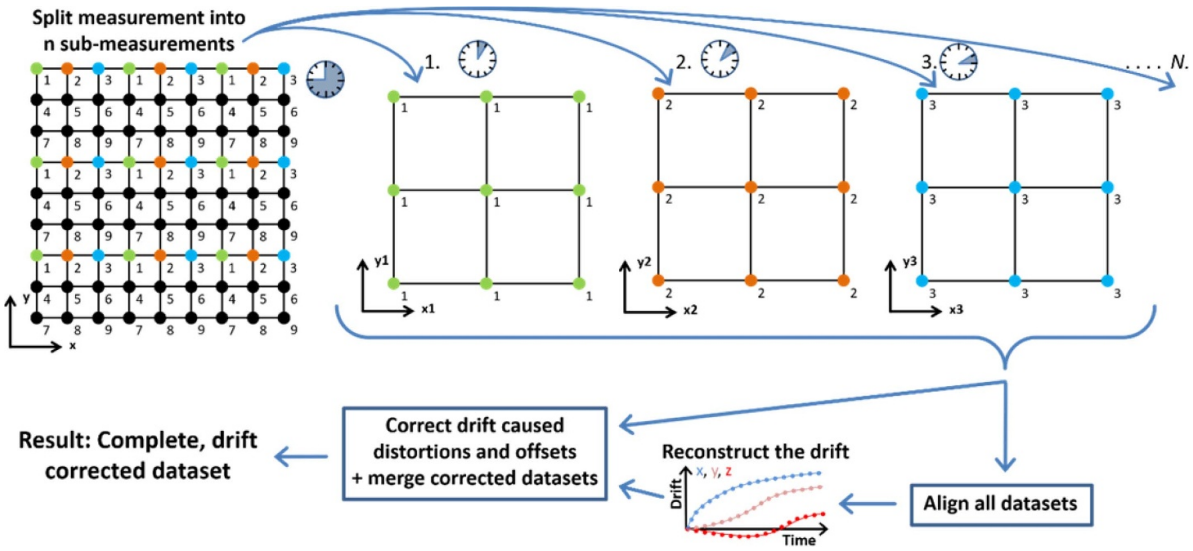

Figure 1. The concept of the new drift-correction method.

expected. For conventional AFM using servo-scanning with almost constant scanning speed, the original image can be split into sub-measurements in a line-wise manner, again with no expected increase in tip wear. For different scanning strategies other splitting approaches can also be realized, as the proposed drift-correction method is not limited to pixel- and line-wise splitting.

Splitting a measurement into sub-measurements yields N datasets that are only slightly distorted by drift because of the reduced measurement time for each dataset. However, the mean drift occurring during two consecutive sub-measurements causes an unknown offset between these datasets. As thermal drift in AFM is normally approximately linear for time scales of some minutes and longer, the unknown offsets between the time-reduced sub-measurements represent a good approximation of the drift rate during these measurements. To determine the unknown drift caused offsets, a point-to-plane ICP algorithm is used.

The point-to-plane ICP algorithm aligns the datasets of the sub-measurements. The alignment of two point clouds using the point-to-plane ICP algorithm is illustrated in figure 2. One point cloud (green) is fixed, while the other one (red) is floating in either 3D (i.e. x-, y- and z-translations) or 6D (i.e. x-, y- and z-translations and three rotations). The functionality of the point-to-plane ICP algorithm is as follows. First, for each point in the floating point cloud, its nearest point in the fixed point cloud is found. For each point in the fixed point cloud, the surface is locally approximated by a plane that is represented by its normal (which can be calculated using the method of Hoppe *et al* [18]), shown as the blue arrows in figure 2(b). The distance of the points in the floating point cloud to the surface planes of the nearest points in the fixed point cloud is determined. Then, a transformation is calculated and applied to move the floating point cloud, so that the summed term of the quadratic point-to-plane distances, which is mathematically expressed in equation (1), is minimized. The point-to-plane distance can be simply calculated by multiplying the x-, y- and z-component of the distance between the two nearest points i (d_x, d_y, d_z) with the corresponding component of the surface normal of the fixed point (n_x, n_y, n_z). By iteratively searching for nearest point pairs and subsequently calculating a transformation for the floating point cloud that minimizes the distance metric of equation (1), the point clouds are aligned closely. As the standard ICP algorithm only aligns two datasets the alignment of all sub-measurements is either carried out sequentially or by using an

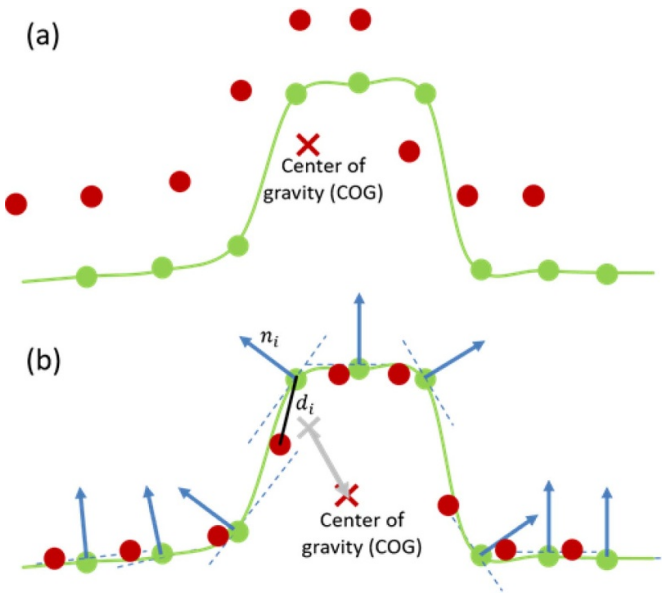

Figure 2. A schematic diagram of point cloud alignment, shown in 2D for the sake of clarity. The green and red points represent the fixed and floating point cloud. The green line represents the sampled surface. The figure is shown as (a) datasets before alignment and (b) datasets aligned using the point-to-plane ICP algorithm.

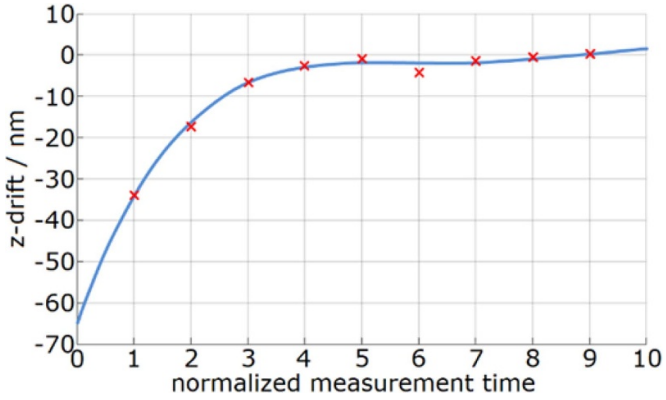

Figure 3. Exemplarily reconstructed z-axis drift during the acquisition of nine sub-measurements. The red crosses mark the mean drift between the datasets determined through the shifts in the COG, and the blue line shows the reconstructed drift function.

extended ICP algorithm that can simultaneously align multiple datasets.

$$dist = \sum_i (d_{x,i} \times n_{x,i} + d_{y,i} \times n_{y,i} + d_{z,i} \times n_{z,i})^2. \quad (1)$$

After the datasets are aligned using the point-to-plane ICP algorithm, the 3D offsets, which indicate the drift, can be calculated as the shift of the center of gravity (COG) of the datasets before and after the alignment. By fitting a polynomial to the temporal course of the drift-caused offsets in the x-, y- and z-axis, respectively, the drift during the sub-measurements is reconstructed. Figure 3 exemplarily shows such a drift curve of the z-axis obtained by nine sub-measurements.

Using the reconstructed drift functions every single datapoint of the (unaligned) datasets is corrected based on the information of its acquisition time, which is either saved during the measurements or approximately derived from the sequence of the point's acquisition. After the correction step the data of the individual sub-measurements are merged into a single dataset. This can be simply done by putting all data points into a single point cloud.

The resulting dataset has significantly reduced drift distortions. This is because of the actual correction process, and because the drift in the initially measured datasets is already reduced due to the shorter measurement time (e.g. due to an averaging effect of residual drift in the final dataset).

The new method offers several advantages. Firstly, the measurement time of a sub-measurement can be almost reduced by a factor of N. It can thus significantly enhance the temporal drift resolution. Secondly, there is no data redundancy. When applying the correction method with line-wise splitting, only small additional travel paths are needed for repositioning the tip on the next scan line. As these motions are usually performed without tip–sample contact they can be performed fast, causing only small increases in the overall measurement time. When applying the correction method with the pixel-wise splitting strategy the additional travel required for positioning the tip over the next sampling position does increase dramatically; however, as this motion is again performed without tip–sample contact it can be performed with high speed, causing only a moderate increase in measurement time. Thirdly, the method is capable of correcting drift in 3D. And finally, it is flexibly applicable to different kinds of surfaces and sampling techniques. As will be demonstrated in this paper later, even very weak surface features available on the sample will be sufficient for aligning the datasets using the point-to-plane ICP algorithm. As the splitting of a measurement can be easily adopted for different scanning and sampling strategies, and because the processing of the data is designed to work with point clouds instead of images, the proposed drift-correction method can also be applied to non-raster scanning AFM [19].

However, the residual drift in the fused dataset causes a slightly increased noise level. Such noise has an amplitude of (far) below 1 nm according to our experience. In addition, the lateral resolution of the fused dataset could be (slightly) worse compared to a single non-split measurement. The reason for this is that unknown offsets between consecutive sub-measurements, either caused by drift itself or by other effects, cause a locally inhomogeneous distribution of the points in the fused dataset. Regularly small areas in the fused dataset are slightly under sampled, which can be interpreted as a loss of lateral resolution.

If the slight degradation of the resolution in the fused dataset is not acceptable, an extended variant of the drift-correction method can be applied. For this variant, the fused and drift-corrected dataset obtained above is used as a reference (A). An additional full resolution measurement of the sample is acquired, leading to a dataset (B). Thus, for the two datasets (A) and (B) obtained, (A) is drift-corrected with slight degradation of resolution, while (B) is drift-distorted but free of degradation of resolution. The extended idea is to combine the datasets (A) and (B) to generate a drift-corrected

dataset without degradation of resolution. To do this, the ICP algorithm is used to align the reference dataset (A) and the drift-distorted dataset (B). After this alignment local deviations between both datasets can be determined. For this, the aligned dataset (B) is divided into multiple segments that may be overlapping. These segments are individually aligned to the reference dataset (A), again using the ICP algorithm. By calculating the shift in the positions of the COG of each segment before and after its alignment, a discrete mapping of the local deviations between both datasets is obtained. Each *x*-, *y*- and *z*-component of the determined local deviations is then fitted to a 2D polynomial function (i.e. a function of drift with respect to the *x* and *y* locations). These *x*-, *y*- and *z*-drift functions are applied to correct the dataset (B). For each point in (B) a correction value for the *x*-, *y*- and *z*-axis is calculated from the drift function using the *x*- and *y*-coordinates of the data points. By correcting the local deviations between the reference dataset (A) and dataset (B), the drift in dataset (B) is corrected to a similar level as in the reference dataset (A) without affecting its noise and resolution. However, the cost of applying this extended variant is the need for doubled measurement time and data redundancy.

3. Implementation

The drift-correction method has been implemented for a new AFM, referred to as a low-noise 3D-AFM, which is currently under development at the Physikalisch-Technische Bundesanstalt (PTB). This AFM has a relatively large measurement chain with a length of about 0.7 m, making it susceptible to drift. To minimize the drift, the AFM is placed in an acoustically and thermally insulated chamber inside a climatized measurement room. After a sufficient waiting time (typically one night) the whole system reaches a stable state, where drift rates are as little as some nm h^{-1}. The AFM is capable of two measurement modes. One is the scanning mode, where the tip is scanned with respect to the sample with a given velocity and the tip–sample interaction is kept constant during scanning. Such a scanning mode is widely applied in almost all AFMs. The needed measurement time is proportional to the total length of the scanning profiles (i.e. the length of profiles times the number of profiles). The other is the so-called VAP [17] measurement mode developed at PTB. Using this mode, the surface is measured point by point. At each point, a tip–sample interaction curve is taken and evaluated for measurements. Compared to the scanning mode, the VAP mode has the advantage of lower tip wear and lower measurement noise and is therefore preferred in our metrology applications. However, the drawback of the VAP measurement is that the measurement time is proportional to the number of pixels to be measured, thus suffering from long measurement times and strong drift. Therefore, in this study, we focus on the application of the proposed drift-correction method on the VAP measurement mode. For ease of operation, our AFM has been designed with an automatic measurement function which can divide a single, complete measurement into sub-measurements, as shown in figure 1.

The software for the offline drift correction has been implemented in an additional software package designed based on the MATLAB® programming platform. For the alignment of the datasets, we use the ICP algorithm implemented by Phillip Glira as part of the freely available 'point cloud tools for MATLAB' [20]. This ICP implementation was originally designed to align aerial laser scanned point clouds [21, 22] and can simultaneously align multiple point clouds. This capability was shown to create more accurate results than the sequential alignment of sub-measured datasets, as is carried out in most ICP-implementations.

After applying the drift-correction method, data points that were originally located on a rectangular grid are no longer present in this strictly regular grid. If the corrected data should be gridded again, we apply a simple linear interpolation. Such interpolation was performed for all the data presented in this paper for improved visibility.

4. Experimental and simulation studies

Both experimental and simulation studies have been carried out to investigate the performance of the proposed drift-correction method. In this paper, we will demonstrate two experimental results and one simulation result as examples.

Figure 4 shows the improvement of the AFM image quality in a measurement scenario with strong nonlinear drift by applying the extended drift-correction method. A line feature is measured over a measurement area of 1800 nm × 1800 nm. A complete image of 181 × 181 data points (i.e. a sampling distance of 10 nm) is first taken. The measurement was performed using the VAP mode with a low probing speed (v = 500 nm s^{-1}), resulting in a long measurement time of approximately 100 min. The obtained AFM image is shown in figure 4(a). It can be seen that the measured line feature appears with a bow on the *z*-axis and a wavelike distortion along the *x*-axis, caused by drift. Then, nine sub-measurements on the same sample area have been performed with 61 × 61 data points (i.e. a sampling distance of 30 nm). Each measurement took 16 min and all sub-measurements 144 min in total. This extra measurement time (44% increase) is owing to the preparation time needed to position the tip to points before VAPs are taken. This extra time can be reduced by increasing the positioning speed without impacting tip wear.

As already detailed in section 2, the nine datasets of the sub-measurements are first fused using the ICP algorithm to generate a complete drift-corrected dataset. This is then applied to correct the full AFM image obtained in the first step. The corrected AFM image of the line feature is shown in figure 4(b). In each of the three coordinate axes of the dataset drift distortions of up to 100 nm were detected (not shown in the figure).

This example qualitatively shows the applicability of the proposed drift-correction method to improving measurements. As can be seen in this example, the quality of the line feature in the corrected AFM image becomes significantly improved.

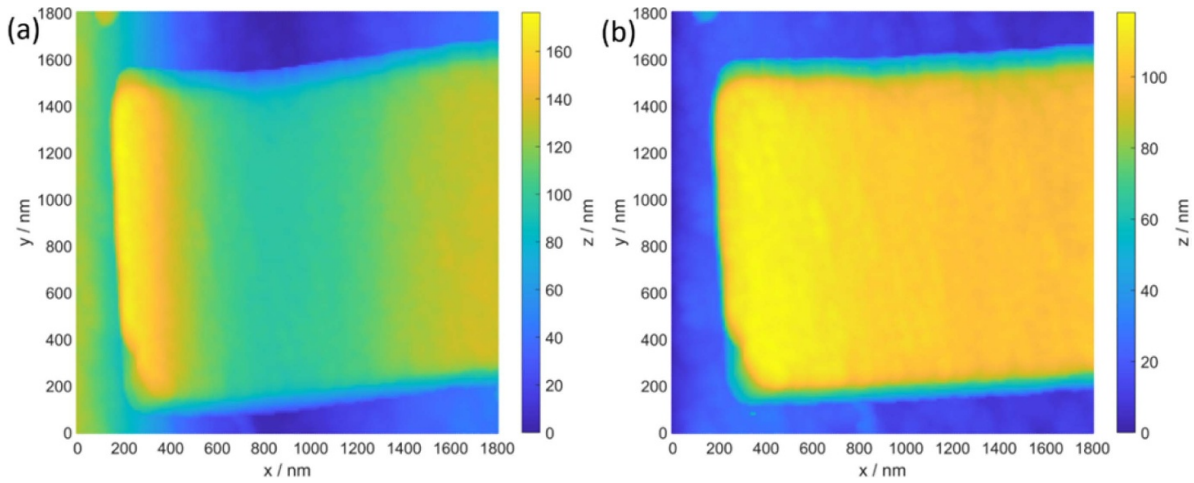

Figure 4. Application of the extended drift-correction method to strongly non-linearly drift-distorted data. (a) Before correction and (b) after correction.

Table 2. A comparison of evaluated pitch values and orthogonality from the measurements with and without the drift-correction method.

Parameters	Day	Measurement (i) without drift correction; *x*-fast measurement axis	Measurement (ii) without drift correction; *y*-fast measurement axis	Measurement (iii) with drift correction
x-pitch (nm)	1	99,67	97,79	99,70
	2	99,66	101,08	99,71
y-pitch (nm)	1	99,56	99,81	99,79
	2	99,62	99,71	99,68
Orthogonality (°)	1	89,29	89,92	89,99
	2	89,57	90,66	90,04

The bow on the *z*-axis and the wavelike distortion along the *x*-axis are (almost) invisible in the corrected image.

To quantitatively investigate the improvements in measurements, the proposed method has been applied in a measurement of a 2D grating with 100 nm nominal pitch. In this experiment, a selected area (2 µm × 2 µm) of the grating is measured in three different ways:

(i) A complete AFM image of the measurement area using the VAP method with 401 × 401 data points (i.e. a sampling distance of 5 nm) using the *x*-axis as the fast measurement axis. The measurement takes 180 min;
(ii) The measurement above is repeated, however, by using the *y*-axis as the fast measurement axis;
(iii) The same grating area is measured in 64 sub-measurements using the VAP method with 50 × 50 data points (i.e. a sampling distance of 40 nm). Each individual sub-measurement takes about 4.5 min (all sub-measurements together consumed 275 min, which is an increase of about 53%).

Figure 5(a) shows a point cloud of one individual sub-measurement; no grating structure is visible due to the large sampling distance. Although a single sub-measurement contains only little information of the sample and all sub-measurements together are offset by drift, the sample surface can be reconstructed using the ICP algorithm and the subsequent correction of the drift. Figure 5(b) depicts a fused drift-corrected AFM image of the grating from 64 sub-measurements.

To illustrate the possible resolution degradation of the fused datasets, we compared two profiles of the grating in figure 5(c) and two small subsets of AFM images in figures 5(d) and (e) for clarity. Figure 5(c) shows the profile from the position marked in figure 5(b) as determined by measurement (i) and by correction and fusion of 64 sub-measurements (iii). Figure 5(d) is a small subset of the fused and drift-corrected dataset (figure 5(b)) at the marked box, while figure 5(e) is a sub-set of the AFM image measured in (i) at the same location. There is almost no resolution degradation visible in the fused dataset.

To quantitatively investigate how the proposed method could improve measurement accuracy, the parameters *x*-pitch, *y*-pitch and orthogonality of the 2D grating are evaluated from both the raw drift-distorted AFM images of the measurements (i and ii) and the fused drift-corrected image of the measurement (iii). All measurements are repeated twice on two different days. The results are summarized in table 2. The evaluation of the data is performed using both the Fourier transformation (FFT-FT) method and the gravity center (GC) method, as published in [23]. As the maximum deviation between the results of the FFT-FT and GC method are only 0.06 nm and the mean magnitude of deviation is as low as 0.023 nm, we list only the results of the FFT-FT method in the table. For both days the

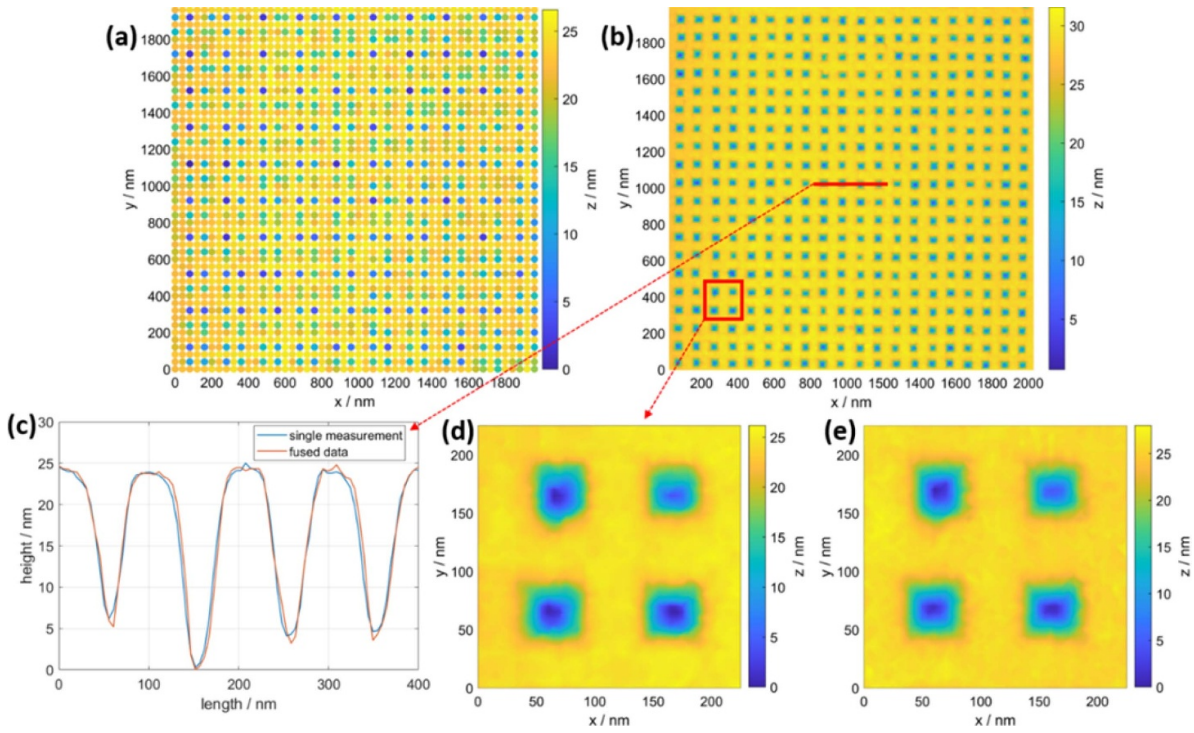

Figure 5. Application of the drift-correction method to a 2D-grating sample. (a) single sub-measurement with 40 nm sampling distance, containing only little sample information; (b) the final drift-corrected fused dataset; (c) comparison of a profile of the grating measured in a single measurement (i) and generated through correction and fusion of 64 sub-measurements (iii); (d) and (e) comparison of a same subset of the fused drift-corrected data and the data acquired in a single measurement. Only little resolution degradation of the drift-corrected dataset can be seen.

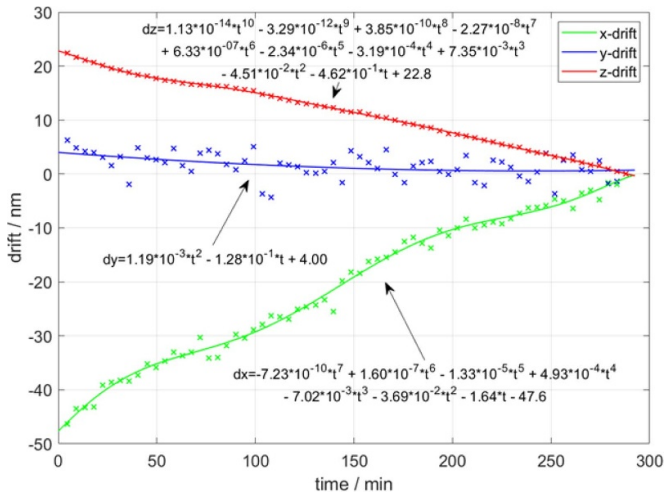

Figure 6. Reconstructed drift from the 64 sub-measurements of the 2D grating on the first day. The crosses represent the offsets of the sub-measurements that were detected using the ICP algorithm and the lines represent the reconstructed drift functions, determined by fitting polynomials to the offset values. The drift in the x- and z-axis could be determined with sufficiently low noise (especially on the z-axis) and, therefore, high-order polynomials are used as correction functions on these axes. On the y-axis the observed drift is quite small; however, it is affected by noise and, therefore, only fitted with a low-order polynomial.

pitch values show the same behavior for the different measurement scenarios.

As can be seen in table 2, the evaluated parameters of two repeated measurements (day 1 vs day 2) of (i) and (ii) show significant deviation, particularly for the results marked in red. It is mainly because these parameters are susceptible to drift and the drifts of two different measurement days might be significantly different, leading to the measurement variations. The pitch values of the fast measurement axes in both measurements (i and ii) are more stable. It is because different parameters are impacted by drift with different time intervals. Taking measurement (ii), which has *a* y-fast measurement axis, as an example, structures along the y-axis can be measured across one profile. Consequently, it is only impacted by the drift at the measurement time interval of one profile. In contrast, the structure along the x-axis suffers from the drift of a time interval of a whole measurement. Similarly, the orthogonality is influenced both by the x-drift and y-drift over the whole measurement time. It should be mentioned that the y-pitch of the measurement (i) has also shown a stable value in two repeated measurements, because the y-drift is quite small compared to the x-drift (figure 6).

Looking at the results of the drift-corrected data, it can be seen that the parameters show high stability in the repeated measurements; only the y-pitch value changes a little due to the fact that not exactly the same surface area was measured on days 1 and 2. Moreover, it can be seen that the drift-corrected x-pitch values agree well with that of measurement (i), while the y-pitch value agrees well with that of measurement (ii). It indicates that the impacts of drift have been greatly corrected in the measurements (iii).

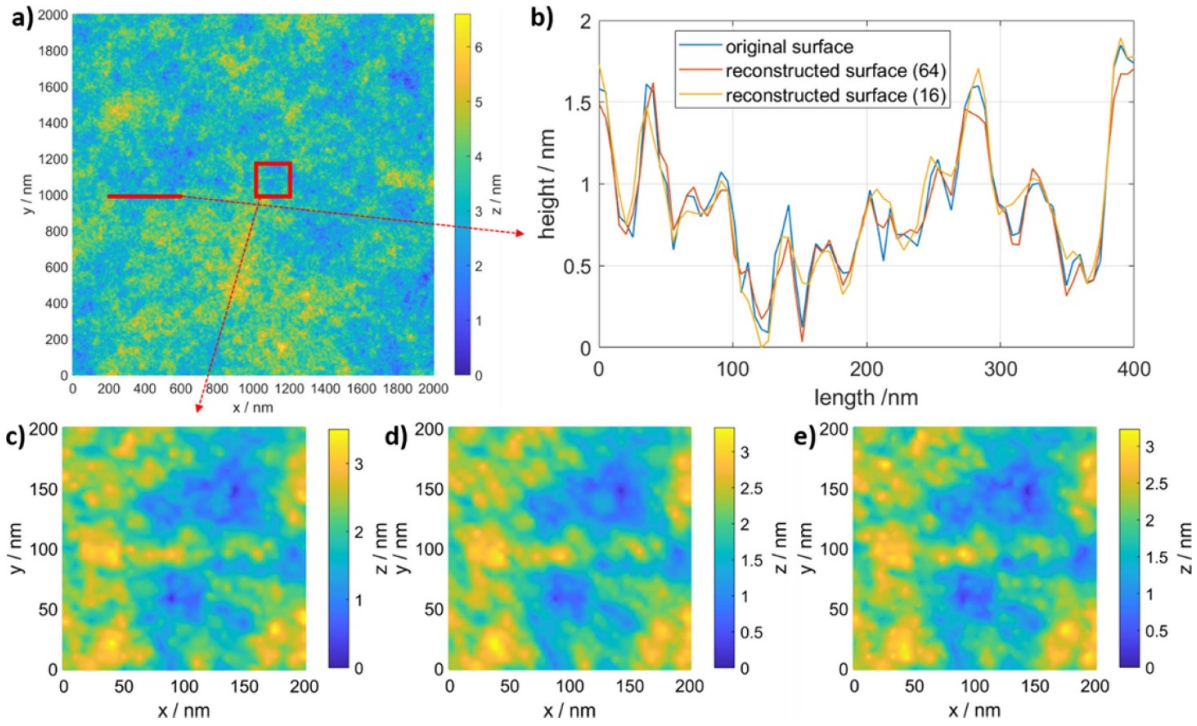

Figure 7. Simulation of the drift-correction method on a rough surface. (a) entire original surface used for the simulation, showing coarse and fine roughness features; (b) comparison of an original surface profile with profiles of reconstructed surfaces using 64 and 16 sub-measurements (note that some of the deviations visible are caused by noise added to the simulation); (c) a small subset of the original surface (S_q of 0.77 nm); (d) a small subset of the reconstructed surface using 64 sub-measurements (S_q of 0.70 nm); (e) a small subset of the reconstructed surface using 16 sub-measurements (S_q of 0.69 nm).

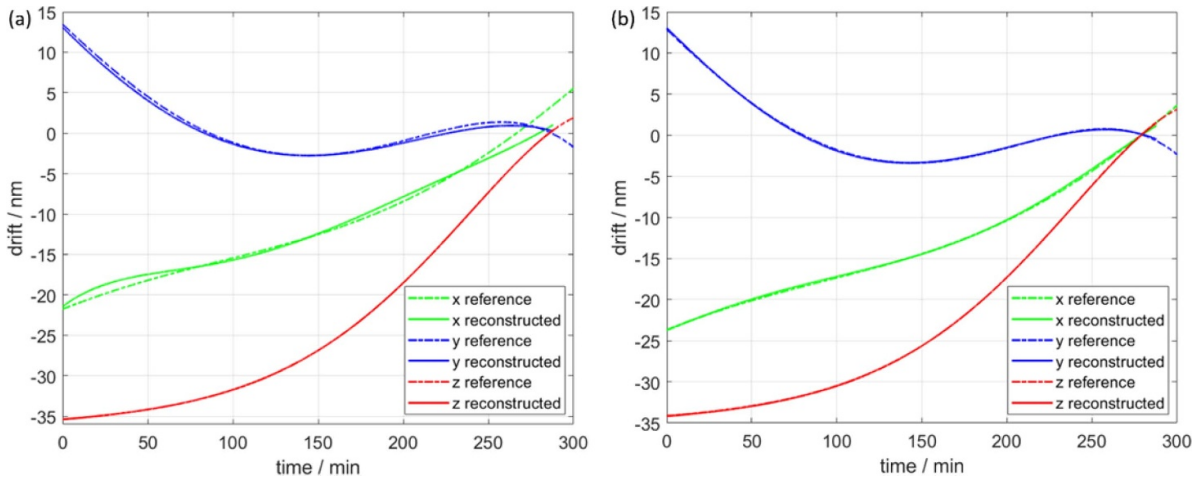

Figure 8. Input drift functions of the simulation and corresponding reconstructed drift functions using (a) 64 sub-measurements and (b) 16 sub-measurements.

As the real drift was not measured in the aforementioned experiments, we cannot evaluate the performance of drift correction precisely. To prove this issue, simulations have been applied. The results of a simulation study are presented as an example. For this, the measurement of a slightly rough surface with a root-mean-square roughness S_q of 0.77 nm, as shown in figure 7(a), has been simulated. The simulated surface consists of fractal roughness, spanning a wide range of length scales. Such a surface represents a typical substrate material of samples. As there is no surface feature with significant geometry, it represents a difficult measurement scenario for the proposed method.

Figures 7(c)–(e) compare a small subset of the reconstructed surface using the drift-correction method and the original surface. As can be seen, the surface could be reconstructed successfully; however, the resolution of the drift-corrected data decreased slightly in this simulation. This is confirmed in figure 7(b) by comparing the

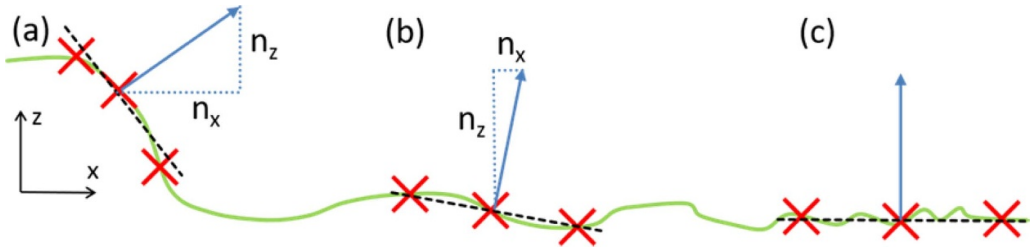

Figure 9. A schematic diagram illustrating the effect of surface topography and sampling distance on calculated surface normals: (a)–(c) represent three different measurement scenarios of a surface with a steep and tall feature, a flat surface with a large wavelength and a flat surface with a short wavelength. In (a), the calculated surface normal has a big component in the x direction. In (b), the calculated surface normal is mainly oriented in the z-direction. In (c), the calculated surface normal cannot represent the real surface normal anymore.

same surface profile of the original and drift-corrected data.

The parameters of the simulated measurement have been chosen in accordance with the real measurement of the 2D grating (64 sub-measurements with 50 × 50 data points, 40 nm sampling density and 4.5 min of measurement time each). To simulate the measurement noise, Gaussian noise with 0.1 nm standard deviation has been added. This noise level again represents the real noise level of our measurement instrument.

Figure 8(a) shows the input drift functions used for the simulation and the respective reconstructed drift. It can be seen that the drift curve can be reconstructed quite well in all three directions. For the z-axis drift, the deviations are significantly less than 1 nm, while for the x- and y-axes the deviation is below approx. 3 nm. It indicates good drift-correction performance using the proposed method, even for such a difficult measurement scenario. The issue concerning the occurred deviations will be discussed in the next section.

5. Discussion

The drift-correction method proposed here has advantages owing to the measurement strategy involving splitting one measurement into N sub-measurements and using the ICP algorithm to align the resulting datasets. The splitting of one measurement into N sub-measurements increases the temporal resolution of the drift correction compared to other 3D drift-correction methods. Generally, the higher N is, the better the temporal resolution. However, a high N will also lead to problems owing to an increased sampling distance in the sub-measurements, which makes accurate data fusion/alignment more difficult. Using the point-to-plane ICP algorithm such difficulty is partially tackled by locally approximating the sampled surface data by planes, resulting in a kind of interpolation effect. However, an optimized number of sub-measurements N still needs to be selected based on e.g. the feature size and the sampling distance of the original measurement, to achieve the maximum correction performance.

The aforementioned point raises a general question regarding the proposed method: which factors do actually impact the performance of the proposed drift-correction method and in what way? We think there are several critical factors, such as the number of sub-measurements N, the sampling distance, the geometry of the sample features as well as the drift itself and the order in which the sub-measurements are taken.

In the following, we shortly present the effect of some of these influence factors. To investigate the influence of the number of sub-measurements N on the drift-correction performance, another simulation has been carried out for the aforementioned simulation study, where N is reduced from 64 to 16. Principally, a high number of sub-measurements yields a higher temporal resolution and lower drift distortion in the individual sub-measurements; however, the reconstructed drift in the simulation shown in figure 8(b) using only 16 sub-measurements is more accurate than that shown in figure 8(a). As can be seen in figure 8(b), by reducing the number of sub-measurements to 16, the drift in all three axes could be determined with an accuracy of below 1 nm. It indicates that for the simulated surface the measurement strategy of figure 8(b) has better balanced parameters (i.e. sampling distance vs the number of sub-measurements). An insight into this phenomenon is discussed below.

In the proposed drift-correction method, the alignment performance of the datasets of sub-measurements using the point-to-plane ICP algorithm is the most critical issue determining the drift-correction performance. The surface normals are of great relevance to the point-to-plane ICP algorithm, as can be understood from equation (1). Thus, they provide an important criterion when choosing the sampling distance in the sub-measurements and, therefore, the number of sub-measurements N. To illustrate this issue, a schematic diagram is given in figure 9, showing the effects of surface topography and sampling distance on the calculated surface normals. For the sake of simplicity, the measurement surface is presented as a profile. Figure 9(a) illustrates a measurement scenario of a surface with a steep and tall feature, while figure 9(b) represents the measurement of a flat surface feature with a large wavelength, and figure 9(c) a flat surface feature with a short wavelength. As can be seen in the figure, the surface normal of the measured data points in (a) has a larger x-component (n_x) than that of (b). From equation (1), it is easily understandable that the ICP algorithm will be more sensitive in aligning the dataset along the x-axis for the measurement scenario (a) than for scenario (b). This fact well explains the impact of the sample topography on the drift-correction performance,

as can be seen in figure 6, where the variation of the determined drift along the *x*- and *y*-axes is much larger than that of the *z*-axis.

Furthermore, figure 9(c) illustrates a measurement scenario where the sampling distance is too large; consequently, the calculated surface normal fails to represent the real surface. It thus leads to deviations in aligning the datasets. This fact well explains the impact of sampling distance on the performance of the drift correction, as shown in figure 8. When N is reduced from 64 to 16, the sampling distance is reduced by a factor of 2. It thus enhances the calculation accuracy of the surface normals, thus also the performance of the point-to-plane ICP algorithm, and finally the performance of the drift correction. This example shows that the criterion for choosing the number of sub-measurements N is the proper representation of the sample point's surface normals. If the distance of the sampling positions in the sub-measurements, which is directly connected to the number of sub-measurements N, is too large to enable the determination of representative surface normals, the number of sub-measurements has to be decreased.

6. Conclusion and outlook

A new, flexible method for correcting 3D non-linear drift of AFMs has been presented. Compared to existing drift-correction methods, the new method is capable of correcting drift in all three coordinate axes with zero data redundancy, little or moderately increased measurement time and great application flexibility and relatively high temporal resolution. However, the method slightly decreases the resolution of the corrected data. For cases where this is not acceptable, an extended variant of the drift-correction method has been introduced, which requires an additional measurement. Experimental and simulation studies have shown the great application capability of the proposed method.

The question concerning the drift-correction performance of the proposed method remains open. In this paper, we discussed some influencing factors such as the number of sub-measurements N, the sampling distance and the geometry of the sample features. However, the question of how an appropriate number N should be chosen is still open and needs to be cleared up in the future. Also, there are other issues needing further study, such as the drift itself and the order of sub-measurements. It is important to thoroughly investigate these issues when selecting the optimal parameters for obtaining the best drift-correction performance. We will further investigate these issues in the future.

In this study, we have focussed on pixel-wise splitting to create the sub-measurements as this is appropriate for our new 3D-AFM, for which drift is a critical issue due to its long measurement time using the VAP mode. The proposed method should also work for normal AFMs using servo-scanning; however, experimental studies need to be carried out in the future.

Acknowledgments

This project has received funding from the Electronic Component Systems for European Leadership Joint Undertaking under Grant No. 826589—MADEin4. This Joint Undertaking receives support from the European Union's Horizon 2020 research and innovation programme and Netherlands, France, Belgium, Germany, Czech Republic, Austria, Hungary and Israel.

ORCID iDs

Johannes Degenhardt https://orcid.org/0000-0001-5508-5556
Gaoliang Dai https://orcid.org/0000-0002-1611-0074

References

[1] Eves B J 2009 Design of a large measurement-volume metrological atomic force microscope (AFM) *Meas. Sci. Technol.* **20** 084003
[2] Korpelainen V, Seppä J and Lassila A 2010 Design and characterization of MIKES metrological atomic force microscope *Precis. Eng.* **34** 735–44
[3] Kizu R, Misumi I, Hirai A, Kinoshita K and Gonda S 2018 Development of a metrological atomic force microscope with a tip-tilting mechanism for 3D nanometrology *Meas. Sci. Technol.* **29** 075005
[4] Weafer P P, McGarry J P, van Es M H, Kilpatrick J I, Ronan W, Nolan D R and Jarvis S P 2012 Stability enhancement of an atomic force microscope for long-term force measurement including cantilever modification for whole cell deformation *Rev. Sci. Instrum.* **83** 093709
[5] Hoogeman M S, Van Loon D G, Loos R W M, Ficke H G, De Haas E, Van der Linden J J, Zeijlemaker H, Kuipers L, Chang M F and Klik M A J 1998 Design and perfor mance of a programmable-temperature scanning tunneling microscope *Rev. Sci. Instrum.* **69** 2072–80
[6] Wang Y, Wang H and Bi S 2014 Real time drift measurement for colloidal probe atomic force microscope: a visual sensing approach *AIP Adv.* **4** 057130
[7] Rahe P, Schütte J, Schniederberend W, Reichling M, Abe M, Sugimoto Y and Kühnle A 2011 Flexible drift-compensation system for precise 3D force mapping in severe drift environments *Rev. Sci. Instrum.* **82** 063704
[8] Yang Q, Jagannathan S and Bohannan E W 2008 Automatic drift compensation using phase correlation method for nanomanipulation *IEEE Trans. Nanotechnol.* **7** 209–16
[9] Marinello F, Bariani P, De Chiffre L and Savio E 2007 Fast technique for AFM vertical drift compensation *Meas. Sci. Technol.* **18** 689–96
[10] Meyer T R, Ziegler D, Brune C, Chen A, Farnham R, Huynh N, Chang J-M, Bertozzi A L and Ashby P D 2014 Height drift correction in non-raster atomic force microscopy *Ultramicroscopy* **137** 48–54
[11] Kizu R, Misumi I, Hirai A and Gonda S 2020 A reference-scan-based method for correcting the nonlinear drift of atomic force microscopy at sub-nanometer precision *Meas. Sci. Technol.* **31** 054009
[12] Rahe P, Bechstein R and Kühnle A 2010 Vertical and lateral drift corrections of scanning probe microscopy images *J. Vac. Sci. Technol.* **28** C4E31–8
[13] Lapshin R V 2007 Automatic drift elimination in probe microscope images based on techniques of counter-scanning and topography feature recognition *Meas. Sci. Technol.* **18** 907–27
[14] Follin N D, Taylor K D, Musalo C J and Trawick M L 2012 Three-axis correction of distortion due to positional drift

in scanning probe microscopy *Rev. Sci. Instrum.* **83** 083711
[15] Chen Y and Medioni G 1992 Object modelling by registration of multiple range images *Image Vis. Comput.***10** 2724–9
[16] Hu Y, Hu S, Su C, Shi J and Ma J 2014 Method and apparatus of operating a scanning probe microscope *US Patent Specification* US 8,646,109 B2 (available at: https://patents.google.com/patent/US8646109B2/en)
[17] Dai G, Hässler-Grohne W, Hueser D, Wolff H, Flügge J and Bosse H 2012 New developments at Physikalisch Technische Bundesanstalt in three-dimensional atomic force microscopy with tapping and torsion atomic force microscopy mode and vector approach probing strategy *J. Micro-Nanolith. MEM* **11** 011004
[18] Hoppe H, DeRose T, Duchamp T, McDonald J and Stuetzle W 1992 Surface reconstruction from unorganized points *Computer Graphics (SIGGRAPH '92Proceedings)* vol 26 pp 71–78
[19] Klapetek P, Yacoot A, Grolich P, Valtr M and Nečas D 2017 Gwyscan: a library to support non-equidistant scanning probe microscope measurements *Meas. Sci. Technol.* **28** 034015
[20] Glira P 2015 Point cloud tools for Matlab (available at: www.geo.tuwien.ac.at/downloads/pg/pctools/pctools.html)
[21] Glira P, Pfeifer N, Briese C and Ressl C 2015 Rigorous strip adjustment of airborne laserscanning data based on the ICP algorithm *ISPRS Ann. Photogramm. Remote Sens. Spatial Inf. Sci.* **2** 73–80
[22] Glira P, Pfeifer N, Briese C and Ressl C 2015 A correspondence framework for ALS strip adjustments based on variants of the ICP algorithm *J. Photogramm. Remote Sens. Geoinf. Sci.* **4** 275–89
[23] Gaoliang D, Pohlenz F, Dziomba T, Xu M, Diener A, Koenders L and Danzebrink H U 2007 Accurate and traceable calibration of two-dimensional gratings *Meas. Sci. Technol.* **18** 415–21